# Preparation of Nickel Aluminum–Manganese Spinel Oxides $Ni_xAl_{1-x}Mn_2O_4$ for Oxygen Electrocatalysis in Alkaline Medium: Comparison of Properties Stemming from Different Preparation Methods

Jilberto Ponce,* Edmundo Ríos,† Jean-Luc Rehspringer,‡ Gérard Poillerat,¶ Pierre Chartier,¶ and Juan Luis Gautier†,[1]

*Departamento de Química, Facultad Ciencias Básicas, Universidad de Antofagasta, Av. Angamos 601, Antofagasta, Chile;
†Departamento de Química de los Materiales, Facultad de Química y Biología, Universidad de Santiago de Chile, Av. L.B.O'Higgins 3363, Santiago, Chile;
‡Groupe des Matériaux Inorganiques. UMR 46 du CNRS, IPCMS, EHICS, 1, rue Blaise Pascal, 67008 Strasbourg, France; and
¶Laboratoire d'Électrochimie et de Chimie Physique du Corps Solide, UMR ULP/CNRS 7512, Faculté de Chimie, Université Louis Pasteur, 1-4, rue Blaise Pascal, 67008 Strasbourg, France

Two different procedures were used to prepare spinel-type $Ni_xAl_{1-x}Mn_2O_4$ ($0 \leq x \leq 1$) compounds to study the effects of solid state properties of mixed oxides on their electrocatalytic properties. The oxalic route, coprecipitation of metal oxalates dissolved in propanol or ethanol, and the propionic route, hydrolysis of metal carboxylates in propionic acid, have been used. In both routes, thermal decomposition produces the corresponding oxides. X-ray diffraction patterns showed that the oxides crystallize in a cubic spinel phase with a unit cell parameter $a$ that increases as aluminum is replaced by nickel. At low $x$ values, compounds prepared by the propionic route showed a larger variation for parameter $a$ than compounds prepared by the oxalic route, probably due to oxygen stoichiometric deficiency. This effect was estimated from the tetrahedral force constant ($k_t$) values, which showed a fast decrease as $x$ varied from 0 to 1. Electrical conductivity, conduction activation energy, hole mobility, and pHz of oxides prepared by the propionic route were also higher than those from oxides prepared by the oxalic route. Crystallinity grade and particle size were nearly 50% higher in propionic-route samples than in oxalic-route samples. The apparent and real electrocatalytic activities of both types of oxides were compared for $O_2$ evolution. © 1999 Academic Press

*Key Words:* manganese oxides; mixed oxides; spinels; sol–gel; electrocatalysis.

## 1. INTRODUCTION

Spinel oxides from transition metals, particularly manganese and nickel spinel phases, are interesting systems because of their electrical and electrocatalytic properties (1, 2), which are based on the presence of two different cationic sites in the spinel structure. For $NiMn_2O_4$, it is assumed that manganese can be located at the tetrahedral and octahedral sites (3–5), although the ionic distribution of manganese cations is not well established. Contrarily, the ionic distribution for cations in $AlMn_2O_4$ spinel phase is $Mn^{2+}[Al^{3+}Mn^{3+}]O_4$ (6). Solid solutions between $NiMn_2O_4$ and $AlMn_2O_4$ are expected to have two manganese valencies in the same oxygen environment. For $Ni_{0.5}Al_{0.5}Mn_2O_4$, the basic ionic distribution is expected to be $Mn^{2+}[Ni_{0.5}^{2+}Al_{0.5}^{3+}Mn_{0.5}^{3+}Mn_{0.5}^{4+}]O_4$. Both conductivity enhancement by electronic hopping (7) and electrocatalytic properties can be explained by the presence of two manganese valencies in the octahedral sites. However, ionic distribution depends not only on cation valencies but also on cation size, polarization, vacancies, pressure, temperature, and, drastically, preparation methods (8).

Oxygen electrode reactions are a useful electrocatalytic feature exhibited by compounds that crystallize with spinel structure. The redox couple $Mn^{4+}/Mn^{3+}$ is a well-known candidate for oxygen electroreduction (9), as in the proposed global reaction $O_2 + 2H_2O + 4e \rightarrow 4OH^-$. On manganese spinels, this reaction is highly sensitive to the number of surface active sites and to the bulk concentration of the $Mn^{4+}/Mn^{3+}$ couple, i.e., to the nature of the other ions present in the structure (10, 11). Therefore, bulk and surface cation distributions must be controlled to prepare compounds with high electrocatalytic reactivity, because they determine the intrinsic factor and real surface area, which, in turn, determine the extrinsic factor. In practice, materials showing high conductivity and high surface area must be selected. In this case, the choice of the preparation method

and thermal treatment are of great importance, because the extension of the real surface area (12, 13) will increase the electrocatalytic surface (14) and will produce important changes in the $M^{3+}/M^{4+}$ or $M^{n+}/M^{(n+1)+}$ ratios (15). As far as series investigation is concerned, intensive comparisons require similarities in preparation techniques, particularly in final heat treatment. Among the various preparation procedures available, e.g., ceramic methods, spray pyrolysis (16), dry evaporation, freeze-drying (17), sputtering (18), and calcination of coprecipitated metal hydroxides (19), the sol–gel method has not been used to prepare mixed oxide electrocatalysts, even though it yields oxides with high surface areas and very narrow particle size distributions (14, 20, 21).

This paper reports the preparation of a $Ni_xAl_{1-x}Mn_2O_4$ series ($0 \leq x \leq 1$) using three different starting preparation methods: precipitation in two different alcohols using oxalates as precursors (oxalic route) and a sol–gel type procedure using a carboxylate polymeric gel in propionic acid as precursor (propionic route). These preparations were expected to render well-defined phases without secondary phases and, therefore, with electrocatalytic activities higher than those of oxides previously prepared by the hydroxide coprecipitation method (19). To evaluate the physicochemical properties of the oxides, samples were characterized by XRD, density, BET specific surface area, electrical conductivity, IR spectroscopy, charge carrier mobility, point of zero charge, and electrode roughness measurements. Preliminary results on the electrocatalytic properties of oxygen evolution on oxides are presented.

## 2. EXPERIMENTAL

### 2.1. Synthesis of $Ni_xAl_{1-x}Mn_2O_4$ Oxides

The chemical synthesis of $Ni_xAl_{1-x}Mn_2O_4$ ($0 \leq x \leq 1$) with $x = 0$, 0.2, 0.35, 0.5, 0.7, 0.8, and 1, was conducted by the oxalic acid route in ethanol or propanol and by the propionic acid sol–gel type route.

*Oxalic acid route.* Ethanolic solutions of $Mn(NO_3)_2 \cdot 4H_2O$ (Merck, Ref. 5940), $Ni(NO_3)_2 \cdot 6H_2O$ (Merck, Ref. 6743), and $Al(NO_3)_3 \cdot 9H_2O$ (Merck, Ref. 1063) were prepared. For example, to prepare 5 g of the composition $Ni_{0.5}Al_{0.5}Mn_2O_4$, 11.58 g manganese nitrate, 3.354 g nickel nitrate, and 4.327 g aluminium nitrate were dissolved in 50 ml of pure ethanol at 60°C. After stirring, 50 ml of an ethanolic solution containing 10.395 g of oxalic acid $H_2C_2O_4 \cdot 2H_2O$ (5% excess to ensure complete precipitation) was added. After a light pink precipitate was formed, 13.5 ml of a 33% ammonia solution was added to neutralize the excess oxalic acid and to precipitate the aluminum hydroxide. After cooling, a white precipitate was obtained. Precipitation completion was tested by adding the precipitating agent to the supernatant liquid. Absence of nickel salt

traces was demonstrated by adding hydroxylamine to the mother solution. The expected stoichiometric cationic ratio was confirmed by atomic absorption analysis. The same procedure was used when solutions were prepared using propanol as solvent. Precipitates were rinsed with water to remove any $NO_3^-$ ions and were dried at 90°C for 24 h before calcination at 1050°C, under Ar atmosphere, for $x = 0$ and $x = 0.2$, and at 950°C under air for the other precipitates with different compositions. TG analyses showed that the spinel phase could be obtained in the temperature range between 800 and 1000°C, depending upon the oxide composition.

*Propionic acid sol–gel type route.* This novel method involved the formation of a viscous gel at 140°C, made up of mixed metal carboxylates, after dissolution of pure manganese carbonate, $MnCO_3$, nickel carbonate hydroxide tetrahydrate, $2NiCO_3 \cdot Ni(OH)_2 \cdot 4H_2O$ (Aldrich, Ref. 33977-6), and aluminum isopropoxide, $Al(C_3H_7O)_3$ (Aldrich, Ref. 22940-7), in pure liquid propionic acid (Janssen, Ref. 149089). Again, for example, to prepare 5 g of the composition $Ni_{0.5}Al_{0.5}Mn_2O_4$, 1.373 g of nickel carbonate, 7.2875 g of manganese carbonate, and 2.9865 g of aluminum isopropoxide were consecutively dissolved in 50 ml of propionic acid. A brownish-green gel was obtained after solvent evaporation, quenched in liquid nitrogen, and further precalcinated at 500°C for 2 h. The final heat treatment was determined by TGA analyses. Manganese carbonate was prepared by adding sodium carbonate, $Na_2CO_3$ (Alfa, Ref. 307528), to concentrated aqueous manganese nitrate solution, $MnNO_3 \cdot 4H_2O$ (Merck, Ref. 5940). The nickel-to-manganese ratios were confirmed by atomic absorption analyses. The final solid obtained was calcined under air (under Ar for $x = 0$ and $x = 0.2$) at the temperatures used in the oxalic acid route.

Finally, all powders obtained by both routes were annealed under air at 500°C for 4 h to achieve thermal equilibrium. The temperature selection was based on the oxides DTG analyses.

### 2.2. Characterization Techniques

Diffractograms were obtained using the powder method with a Philips 1050–80 diffractometer and $CoK\alpha$ radiation. A Jeol (JSM 840) SEM apparatus was used to obtain scanning electron microscopy photographs. Thermogravimetric and differential analyses were performed in a TG-DTA Setaram apparatus. BET specific surface areas ($S_g$) for $Ni_xAl_{1-x}Mn_2O_4$ series ($0 \leq x \leq 1$) powders were obtained with a Carlo Erba instrument (Sorpty 1750) using nitrogen gas. Density measurements were carried out in a helium pycnometer from Quantachrome Co. Oxidation power ($q$) was determined by chemical reduction of $Mn^{n+}$ cations, with $n \geq 3$, using 0.9830 N $VOSO_4$ as a soft reducing agent.

In this method, which has been widely used by us (10, 11. 22), approximately 600 mg of oxide was mixed with 30 ml of $VOSO_4$ and 20 ml of 2.4 M $H_2SO_4$ (to avoid $MnO_2$ formation) and the mix was heated at 80°C for 48 h. After oxide dissolution, the $VOSO_4$ excess was potentiometrically titrated with 0.9860 N $KMnO_4$ solution, prepared and standardized according to McBride's method (23). Oxidation power was calculated according to the equation

$$q = \frac{(V_{VO}N_{VO} - V_K N_K) M_{ox}}{m_{ox}},$$

where $V_{VO}$ and $N_{VO}$ and $V_K$ and $N_K$ are the volume and concentration of $VOSO_4$ solution and $KMnO_4$ solution, respectively, $M_{ox}$ and $m_{ox}$ corresponding to molar mass and weight of oxide. Each determination was made at least three times. The standard deviation, considering all experimental measurements, was estimated to be $\pm 0.02$. Oxygen stoichiometry was determined in an induction furnace with stabilized zirconia as oxygen sensor (LECO TC 136 apparatus). A 20-mg pellet sample was put in a crucible, containing Ni as catalyst, and it was heated until complete oxide calcination. Released oxygen was carried away toward the sensor by Ar gas flow. The measurement had an accuracy of 0.2%.

Electrical conductivities of Ni–Al–Mn oxides were measured in a Keithley 2207 ohmmeter in the 25–600°C temperature range, using heating–cooling cycles. The powders were compressed at 2.5 ton $cm^{-2}$ into a parallelepipedic shape ($15 \times 2 \times 5$ mm) and were painted with silver paint to ensure ohmic contacts.

To determine major optical absorption vibrations, transmission infrared spectra were recorded in a FTIR spectrophotometer (Bruker IFS 66), between 400 and 4.000 $cm^{-1}$, in KBr (4 $cm^{-1}$ resolution).

The pH of zero charge, pHz, of the oxide powders was determined by equilibrium potentiometric titration technique in 0.1 M $KNO_3$ solution, using a gas-tight cell, continuously purged with high-purity $N_2$ to avoid $CO_2$ contamination. The oxide powder was immersed in the previously degassed $KNO_3$ solution and adjusted to alkaline pH. The dispersion was left to equilibrate for at least 1 h before it was titrated by adding fixed volumes (20 μl) of 0.1 M KOH or HCl, with a waiting period of 3 min between titrant additions. Isoelectric points (i.e.p.) were estimated from electrophoretic measurements, using a Zeta-meter Inc. ZM-77 apparatus. Briefly, oxide powders were suspended in $10^{-3}$ M KCl aqueous solution, at alkaline or acid pH, using KOH or HCl diluted solutions, respectively, and zeta potential ($\zeta$) was measured as a function of pH.

Electrochemical characterization was performed in 1 M KOH solutions using stationary and cyclic voltametry in a thermostated three-compartment all-glass cell at 25 $\pm$ 1°C. Electrode potentials were referred to a Hg/HgO/1 M KOH electrode ($E = 0.098$ V/SHE). Intensities of capacitive currents from cyclic voltammetry measurements, in Ar-saturated 1 M KOH solution, were used to estimate the porous pellet electrodes roughness factor, Rf. We tested scan rates ($v = dE/di$) from 1 to 4.5 V $min^{-1}$ in a small potential range ($-0.04$ to $+0.04$ V) free of faradaic currents. Double layer capacitance values were determined from the slope of a linear plot $i_{cap}$ vs $v$ ($C = i_{cap}/v$), where $i_{cap}$ corresponds to the charging current measured at midscan rate (i.e., 0.0 V). The capacitance obtained was compared to a reference value of $C^* = 60$ μF $cm^{-2}$, which corresponds to an ideal oxide electrode (Rf = 1) (24): Rf = C/60. Voltammetric curves were recorded using a Pine RD3 potentiostat and a XY recorder (Houston 2000). Pellet electrodes were manufactured according to the Teflon-bonded method, using graphite (UCAR, Union Carbide) as a conductivity additive (25, 26). To form a paste, wet powder oxides (325 mesh), in isopropylic alcohol, were mixed with graphite, in a ratio of 15:85 (w/w). The paste was mixed with Teflon (Dupont), in a ratio of 10:3 (w/w), followed by a thermal treatment at 350°C under Ar. Pellet electrodes were prepared by pressing the powder into 13-mm-diameter pellets at 5 ton $cm^{-2}$. Ohmic contacts were made of silver paint and isolated from solution with Araldite glue.

## 3. RESULTS

### 3.1. Materials Characterization

*X-ray diffraction analysis.* An X-ray diffractogram for $Ni_x Al_{1-x} Mn_2 O_4$ ($1 \geq x \geq 0$) prepared by the sol–gel route is shown in Fig. 1. Good crystallinity and absence of secondary phases can be observed. Crystallinity varied among members of the series. Diffractograms for $x = 0.2$ and $x = 0.35$ showed peaks broader than those from other oxides, denoting the effect of aluminum substitution by nickel, at low concentration. Cell parameters and $\langle hkl \rangle$ indices were computed in a Lattice program (27). Oxides prepared by the oxalic route showed classical spinel diffractograms. Examples belonging to the $Fd3m$ symmetry are shown in Fig. 2. The cubic cell parameter $a$ increased with nickel ratio $x$, as expected (Fig. 3). An even more pronounced enhancement can be observed with the propionic route. Standard deviation for $a$-cell determinations was lower than $\pm 0.0005$ nm.

*Scanning electron microscopy.* Microphotographs for oxides prepared by propionic and oxalic routes at two nickel concentrations, $x = 0.35$ and $x = 1$ are shown in Fig. 4. Compared with oxide prepared by the oxalic route, propionic-route compounds are more homogeneous and showed a very narrow particle size distribution, around 0.5–0.8 μm for $x = 0.35$ (Fig. 4B) and 0.9–1.3 μm for $x = 1$ (Fig. 4A). The grain size of propionic-route samples
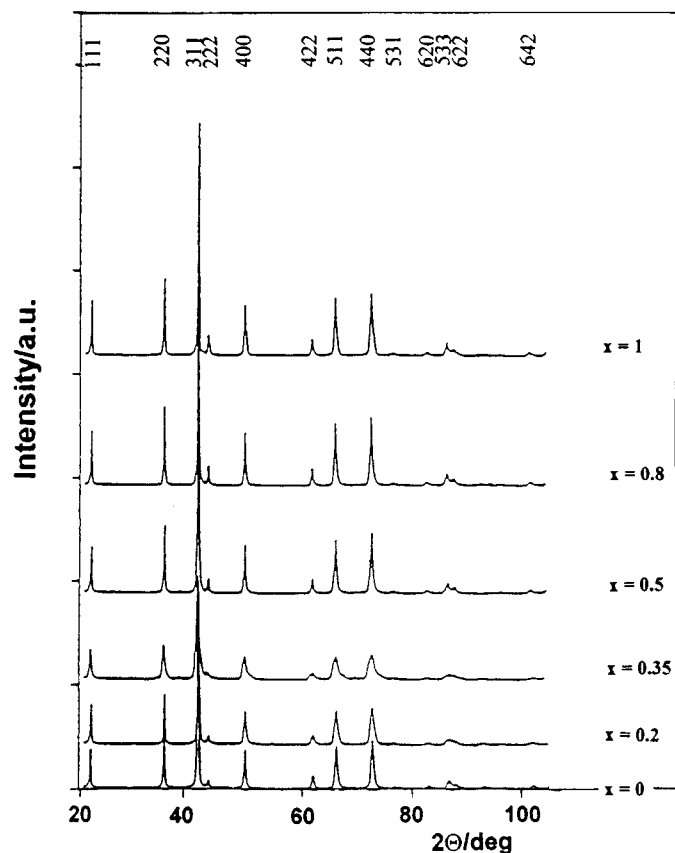
**FIG. 1.** X-ray diffractograms from oxides prepared by the sol–gel method.

appeared to be about 50% higher than that of oxalic-route samples. Higher grain size values are obtained at high *x*-values, supporting the influence of oxide composition on grain size. Pellet electrodes manufactured with sol–gel compounds showed higher porosity and lower surface area than those made from powders prepared by the oxalic route. In fact, specific surface area measurements using the BET method showed that propionic-route oxides have specific area, Sg, ranging from 1 to 4 $m^2 g^{-1}$, whereas the Sg values for oxalic-route preparations were between 1 and 10 $m^2$ $g^{-1}$. Low Sg values are normally expected for samples annealed at high temperature (14).

*Density measurements and oxidation power.* Density values varied from 4 to 5 $g cm^{-3}$ with both methods, increasing with their nickel content. Low nickel contents produced low density values, probably due to non-stoichiometry in oxygen, as exemplified in Table 4 for propionic route oxides $Ni_xAl_{1-x}Mn_2O_{4-\delta}$. For $x \geq 0.5$, they were stoichiometric in oxygen ($\delta = 0$), but for $x = 0.0$, 0.2, and 0.35, $\delta = 0.1$, 0.08, and 0.05, respectively. This nonstoichiometry condition affects the oxide's oxidation

power: the equivalent amount per oxide mole, $q(x)$, increased with $x$. This suggests that progressive replacement of $Al^{3+}$ ions by $Ni^{2+}$ ions at the B octahedral sites would generate $Mn^{4+}$ ions from $Mn^{3+}$ ions. The preparation method used seems to have no important effect on the metal oxidation state. Thus, $q$ values for oxalic-route and propionic-route preparations increased from 1.1 to 2.0 and from 1.0 to 2.0, respectively, as composition changed from $x = 0$ to $x = 1$.

*Electrical conductivity.* A 10-fold increase in electrical conductivity was observed when $x$ changed from $x = 0.4$ ($4 \times 10^{-9} S cm^{-1}$) to $x = 0.7$ ($5 \times 10^{-8} S cm^{-1}$), demonstrating the effect of Ni incorporation into the spinel structure. The propionic route yielded pure oxide pellets with



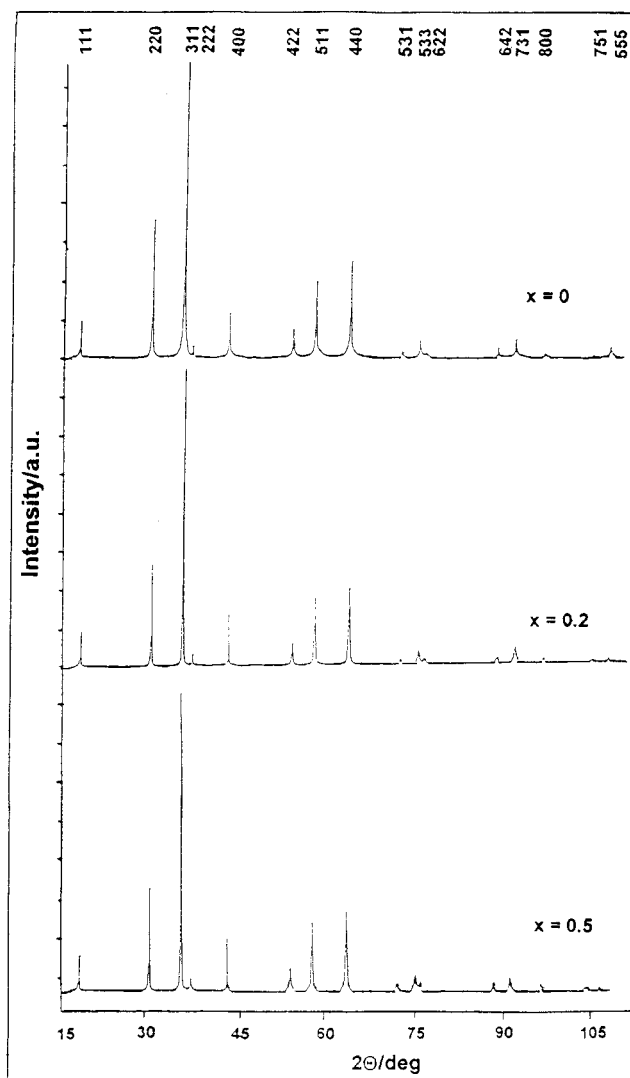**FIG. 2.** X-ray diffractograms from oxides prepared by the oxalic method.
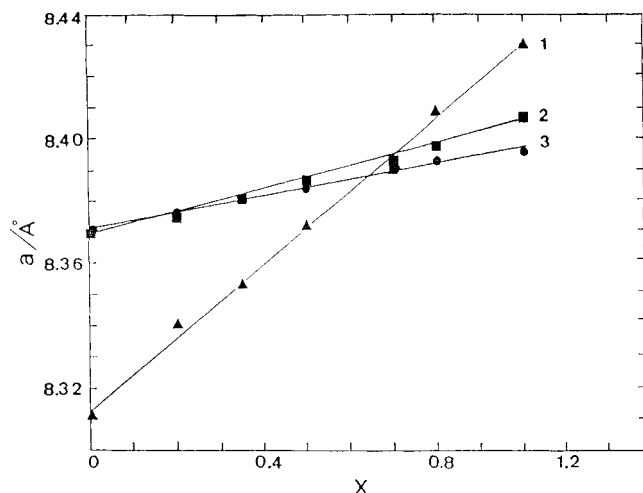
**FIG. 3.** Lattice parameter (a) values as a function of composition ($x$) for $Ni_xAl_{1-x}Mn_2O_4$ oxide system prepared by (1) propionic route, (2) oxalic-ethanol route, and (3) oxalic-propanol route.

higher conductivities than those obtained by the oxalic route for values between $x = 0.4$ and $x = 1.0$. Conductivity, $\sigma$, increased exponentially with $T$, as expected from the Arrhenius law for semiconductors, $\sigma = \sigma_0 \exp(-E_a/kT)$, where $E_a$ is the activation energy for the conducting process. Based on the Seebeck effect, all oxide samples prepared in this study showed an $n$-type semiconducting character. The $E_a$ values measured for the oxide pellets are shown in Fig. 5. These were obtained as a function of both oxide composition and preparation method. At low $x$ values, $E_a$ was very similar for both methods. At high nickel concentrations, however, the propionic route showed higher $E_a$ values. These results may be connected with charge carrier mobility values (see below).

*IR spectroscopy.* Table 1 provides the IR band position for each characteristic frequency, $v_1$ and $v_2$, as a function of both oxide composition and preparation method. The band energy decreased when $x$ increased, and propionic-route products showed higher energies than oxalic-route compounds.

The mobility of the charge carriers ($\mu$) can be deduced from frequency values ($v_1$), lattice parameters ($a$), and activation energies ($E_a$), according to Hiekes and Johnston [28]: $\mu = ed^2v_1 \exp(-E_a/kt)/kt$, where $d$ is the jump distance between nearest neighboring B-sites ($d = 1/4a\sqrt{2}$). The variation of computed mobilities with composition is shown in Fig. 5, together with the experimentally measured corresponding activation energies, $E_a$. Clearly, $E_a$ decreases when $\mu$ increases.

Applying Waldron's theory to cubic spinels (29), we were able to determine the octahedral ($k_0$) and tetrahedral ($k_t$)

force constants, based on the frequencies of the two strongest IR bands obtained. Absorption band $v_1$ corresponds to metal–oxygen (M–O) longitudinal vibrations and the metal cation is octahedrally coordinated, while the $v_2$ band is assigned to a vibration involving the $M^{3+}$ cation in either an $[MO_4]$ tetrahedron or a $[MO_6]$ octahedron (30). The corresponding relationships are
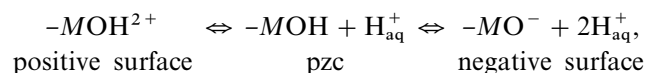
$$k_{oc} = \frac{(2\pi c)^2 M_{oc}M_x}{N(4M_x + M_{oc})} v_2^2 \qquad [1]$$

$$k_t = \frac{(2\pi c)^2 M_t v_1^2}{N4(1/3 + 1/\tau)}. \qquad [2]$$

Subscripts oc and t are related to octahedral and tetrahedral sites, $N$ is Avogadro's number, $c$ is the speed of light, $\tau$ is the tetrahedral cation's relative shift, $M_x$ is oxygen's molecular weight, $M_{oc} = xM_{Ni} + (1-x)M_{Al} + M_{Mn}$, and $M_t = M_{Mn}$, with $M_{Ni}$, $M_{Al}$, and $M_{Mn}$ being the Ni, Al, and Mn molecular weights and assuming an atomic distribution $Mn[Ni_xAl_{1-x}Mn]$. Table 1 shows the force constant values. For the range $x = 0.35$ to $x = 0.5$, elastic $k_{oc}$ and $k_t$ constants exhibited maximum and minimum values, respectively, in agreement with the ionic structure modification in which the $Mn_A^{2+}$ and $Mn_A^{3+}$ concentrations decrease but the $Mn_B^{3+}$ concentration increases. Also, for $x \leq 0.35$ (sol–gel oxides) $k_t$ will increase as the $Mn^{2+}$–O distance decreases, due to a decrease in manganese concentration at the A-site.

### 3.2. Oxide Surface/Solution Measurements

$H^+$ and $OH^-$ ions play a potential-determining role in charging the oxide/solution double layer. The effect of pH may be represented as

$$-MOH^{2+} \quad \Leftrightarrow \quad -MOH + H_{aq}^+ \Leftrightarrow \quad -MO^- + 2H_{aq}^+,$$
$$\text{positive surface} \qquad \text{pzc} \qquad \text{negative surface}$$

where $M$ is a surface cation. Point zero charge, pzc, can be expressed in terms of pH as $pHz = -\log a_{H+,z}$, where $a_{H+,z}$ is the activity of hydronium ions for zero surface charge. Table 2 shows the pHz and i.e.p., values as a function of $x$. As nickel content increases, both pHz and i.e.p., values decrease in different magnitude. The i.e.p. values are lower than the pHz values, probably due to specific adsorption of ions, particularly $Cl^-$, from the electrolyte. Clearly, the surface of the oxide is saturated with a carpet of OH groups, since water molecules adsorbed on surface cations would further transfer a proton to a neighboring oxygen atom at the oxygen sublattice. These OH groups will mediate the interaction between the surface of the oxide and the environment. Because surface structure controls the oxide's electrocatalytic activity, the importance of pHz lies
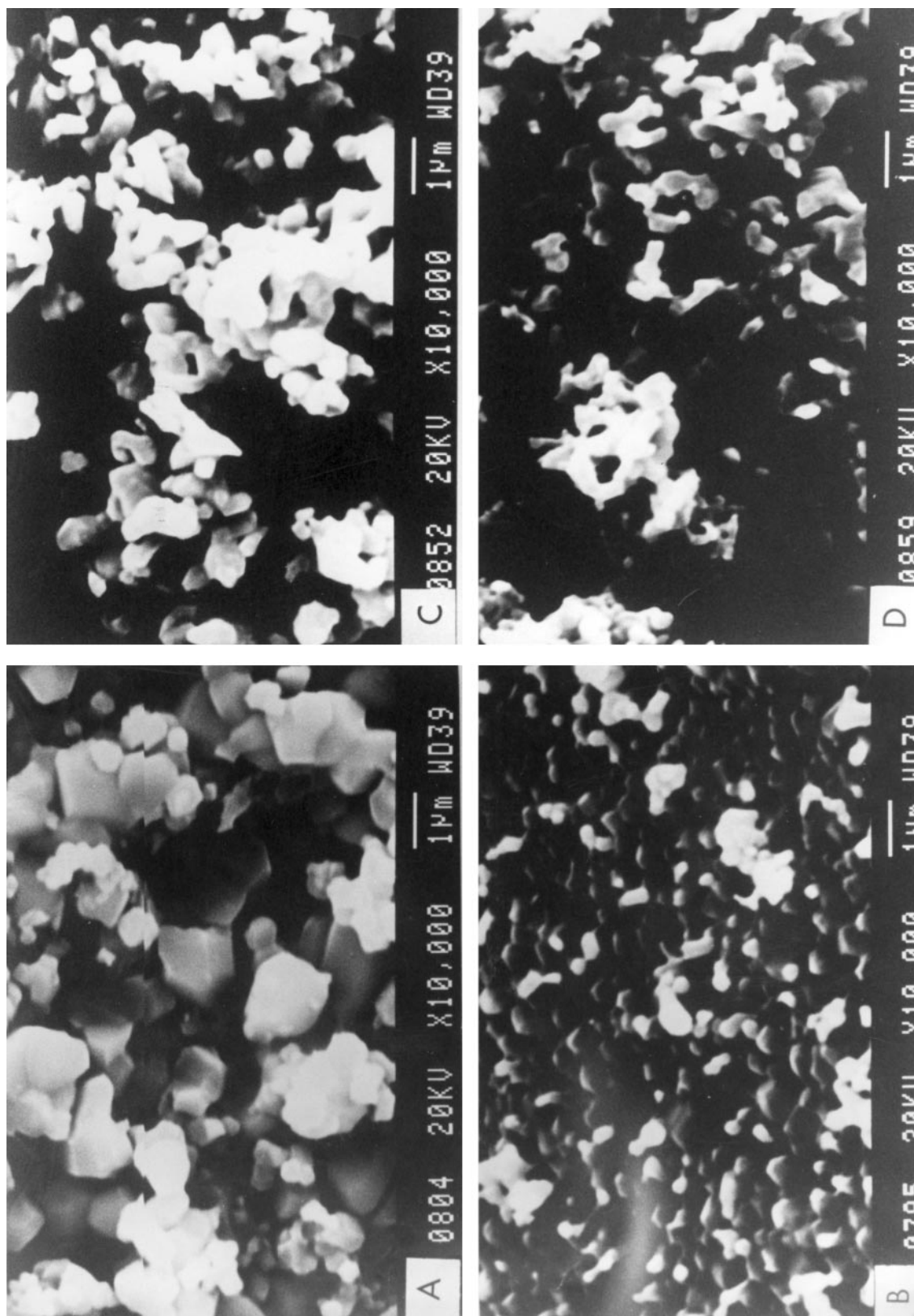
**FIG. 4.** S.E.M. for oxides prepared by the propionic route (A: $x = 1$; B: $x = 0.35$) or the oxalic route (C: $x = 1$; D: $x = 0.35$).
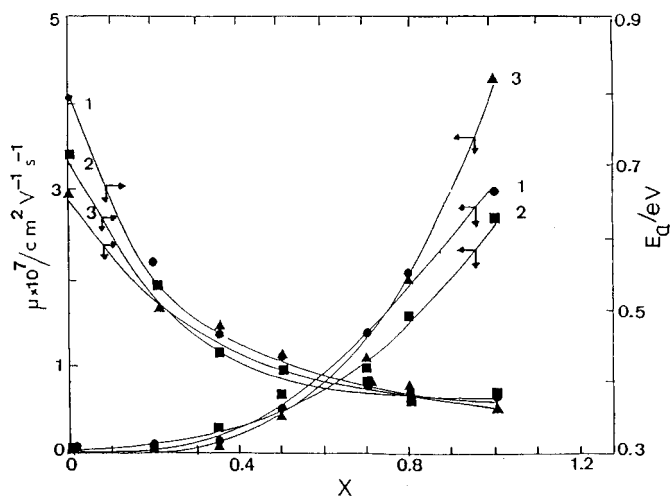
**FIG. 5.** Carrier charge mobility ($\mu$) and conduction activation energy $E_a$ as a function of $x$ values for $Ni_xAl_{1-x}Mn_2O_4$. (1) Oxalic-propanol route; (2) oxalic-ethanol route; (3) propionic route. Pellet thickness: 5 mm.

in its sensitivity to surface structures. We have proposed a correlation between the pHz and the Tafel slopes for the electrocatalytic oxygen evolution reaction (11).

**TABLE 1**
**Transmission IR Results from $Ni_xAl_{1-x}Mn_2O_4$ Prepared by Propionic and Oxalic Routes**

| $x$ | $v_1$ (cm$^{-1}$) | $v_2$ (cm$^{-1}$) | $10^{-5}k_t$ (dyn cm$^{-1}$) | $10^{-5}k_o$ (dyn cm$^{-1}$) |
|---|---|---|---|---|
| | | Propionic route | | |
| 0 | 639 | 486 | 1.81 | 1.25 |
| 0.2 | 620 | 485 | 1.60 | 1.29 |
| 0.35 | 615 | 484 | 1.54 | 1.31 |
| 0.5 | 609 | 480 | 1.50 | 1.31 |
| 0.7 | 607 | 473 | 1.52 | 1.30 |
| 0.8 | 606 | 464 | 1.55 | 1.27 |
| 1 | 603 | 456 | 1.56 | 1.25 |
| | | Oxalic-propanol route | | |
| 0 | 628 | 491 | 1.64 | 1.28 |
| 0.2 | 619 | 487 | 1.55 | 1.30 |
| 0.35 | 615 | 484 | 1.53 | 1.30 |
| 0.5 | 612 | 470 | 1.56 | 1.26 |
| 0.7 | 610 | 467 | 1.55 | 1.27 |
| 0.8 | 603 | 462 | 1.50 | 1.26 |
| 1 | 602 | 457 | 1.52 | 1.60 |
| | | Oxalic-enthanol route | | |
| 0 | 629 | 492 | 1.65 | 1.29 |
| 0.2 | 624 | 486 | 1.64 | 1.27 |
| 0.35 | 617 | 481 | 1.57 | 1.28 |
| 0.5 | 610 | 479 | 1.49 | 1.31 |
| 0.7 | 608 | 468 | 1.52 | 1.28 |
| 0.8 | 605 | 463 | 1.52 | 1.27 |
| 1 | 603 | 453 | 1.55 | 1.24 |

**TABLE 2**
**pHz and i.e.p., Values for $Ni_xAl_{1-x}Mn_2O_4$ Oxides as a Function of $x$ Values**

| $x$ | Oxalic-ethanol | | Propionic | | | |
|---|---|---|---|---|---|---|
| | pHz | i.e.p. | pHz | i.e.p. | $C_{app}$ ($\mu$F cm$^{-2}$) | Rf |
| 0 | 8.4 | 6.8 | 9.9 | 7.4 | 1408 | 23 |
| 0.2 | 7.9 | 6.4 | 9.6 | 7.2 | 1100 | 18 |
| 0.35 | 7.6$_5$ | 6.0 | 9.1 | 7.0 | 1040 | 17 |
| 0.5 | 7.6 | 5.9 | 8.1 | 6.6 | 847 | 14 |
| 0.8 | 7.2 | 5.5 | 7.7 | 6.0 | 629 | 11 |
| 1 | 6.8 | 5.9 | 7.6 | 5.8 | 575 | 9 |

*Note.* Apparent capacity and roughness factor values are also shown for propionic-route pellet electrodes.

As a test for electrocatalytic activity, we have used the oxygen evolution reaction (OER) from KOH solutions, which occurs according to the global reaction $4OH^- \rightarrow O_2 + 2H_2O + 4e^-$. Figure 6 shows the apparent current densities for the propionic Ni–Al mixed oxides investigated. Both interfacial capacity and roughness factor decrease as $x$ values increase (Table 2). The apparent reactivity measured by the Tafel slope, $b$ (from $E = a + b \log j$), showed a similar dependence on $x$. Tafel slopes obtained from overpotential $\eta$–log $j$ graphs, based on real current densities, are shown in Table 3. Corrections were considered for Rf and graphite contributions to the electrocatalytic current. Clearly, $b$ values decreased with increments in the $x$ values, without important contributions from the preparation method used.
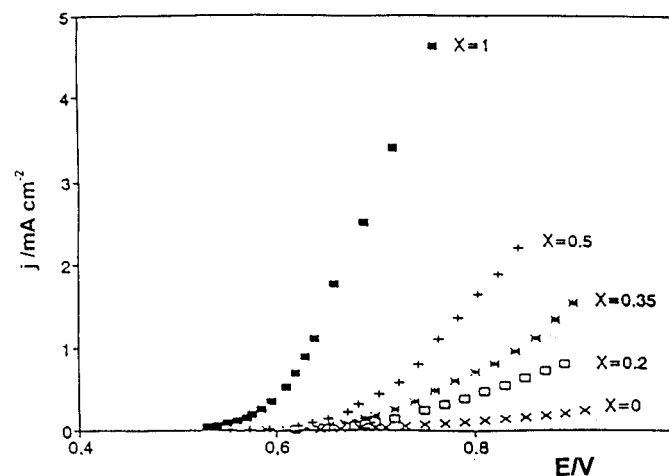


**FIG. 6.** Effect of $x$ values on OER evolution rates from aqueous 1 M KOH solutions at 25°C, expressed as current density $j$ (in mA cm$^{-2}$) on a $Ni_xAl_{1-x}Mn_2O_4$ rotating disk electrode (3000 rpm) prepared by the propionic route.

**TABLE 3**
**Tafel Slope Values for Oxygen Evolution Reaction as a Function of $x$ Values and Preparation Method**

| $x$ | Oxalic route $b$ (mV dec$^{-1}$) | Propionic route $b$ (mV dec$^{-1}$) |
|---|---|---|
| 0 | 121 | 120 |
| 0.2 | 87 | 97 |
| 0.35 | 85 | 87 |
| 0.5 | 70 | 85 |
| 1 | 66 | 68 |

## 4. DISCUSSION

The syntheses of the compounds under investigation using the ceramic method require high temperatures, 1100°C for NiMn$_2$O$_4$, starting from NiO + Mn$_3$O$_4$ (31), and 1500°C for AlMn$_2$O$_4$, starting from Al$_2$O$_3$ + Mn$_3$O$_4$ (32), and very long thermal treatments (several days). In air, thermal decomposition of coprecipitated oxalate precursors, (Ni$_x$Mn$_{1-x}$)C$_2$O$_4 \cdot$ 2H$_2$O, initially leads to a mixture of Mn$_2$O$_3$ and NiMnO$_3$ phases. Ni$_x$Mn$_{3-x}$O$_4$ solid solutions can only be obtained at 800°C, under pure N$_2$ (33). The new preparation method reported here decreases the elaboration temperatures by 200 or 400°C and shortens also annealing time (8 and 3 h) for the oxalic and propionic routes, respectively. The materials show good crystallinity and are free of parasitic phases. The lattice parameter $a$ increases with $x$, as it could be predicted in accordance with the nickel–aluminum substitution. Propionic-route samples with $x < 0.35$ showed $a$ values lower than expected, probably as a result of vacancies at the oxygen sublattice. Electronic conduction increased with $x$, due to the changes in the Mn oxidation state. To explain the electric conductivity of mixed manganese oxides, Ghare $et$ $al.$ (7) considered a hopping mechanism for the charge carriers between Mn ions having the same coordination degree as oxygens in the structure. With this in mind, AlMn$_2$O$_4$ and NiMn$_2$O$_4$ would exhibit higher and lower $E_a$ values, respectively, considering the cationic distribution proposed in the literature, Mn$^{2+}$[Al$^{3+}$Mn$^{3+}$]O$_4$ ($a$ = 0.8312 ± 0.0003 nm 34) and Ni$_{0.35}^{2+}$Mn$_{0.65}^{2+}$[Ni$_{0.65}^{2+}$Mn$_{0.7}^{3+}$Mn$_{0.65}^{4+}$]O$_4^{2-}$ (3, 5). Even though Mn$^{3+}$ cations have a strong preference for octahedral sites, an alternative cation distribution, Mn$_{0.65}^{2+}$Mn$_{0.35}^{3+}$ [Ni$^{2+}$Mn$_{0.35}^{3+}$Mn$_{0.65}^{4+}$]O$_4^{2-}$, has been suggested (31). In AlMn$_2$O$_4$, replacement of Al by Ni should lead to Ni$^{2+}$ or Ni$^{3+}$. A redox process between Ni(III) and Mn(III), leading to increments of Mn$^{4+}$ concentration at B-sites, has been considered to account for the electrical properties of NiMn$_2$O$_4$ (35). Considering the electrical conduction and to ensure electrical neutrality, oxidation of Mn$^{3+}$ to Mn$^{4+}$ at octahedral B-sites, or Mn$^{2+}$ to Mn$^{3+}$ at tetrahedral A-sites,

may be assumed and would take place when Al was substituted by Ni, although it is theoretically difficult to admit the persistence of cubic symmetry for the later case. The distribution Mn$^{2+}$[Al$_{1-x}^{3+}$Ni$_x^{2+}$Mn$_{1-x}^{3+}$Mn$_x^{4x}$] O$_4$ would certainly explain both conductivity enhancement and sign of the charge carriers, but a constant Mn$^{2+}$ concentration at A-sites is excluded, considering the $k_t$ determinations in this work, since $k_t$ values from Mn$^{2+}$–O bonds at A-sites decrease with $x$.

### Cationic Distribution for Ni$_x$Al$_{1-x}$Mn$_2$O$_4$ $(0 \leq x \leq 1)$

A refined general formula for Ni$_x$Al$_{1-x}$Mn$_2$O$_{4-\delta}$ cation distribution, depending upon variables $x$ and $y$ and considering nonstoichiometry, can be expressed as Ni$_y^{2+}$Mn$_{1-y}^{2+}$[Al$_{1-x}^{3+}$Ni$_{x-y}^{2+}$Mn$_{1+2y-x}^{3+}$Mn$_{x-y}^{4+}$]O$_{4-\delta}^{2-}$. This ionic distribution was obtained using the invariant character proposed by Poix (36) for the cation–oxygen distance in his study of AB$_2$O$_4$ spinel structures. Distances at sites A and B are functions of both the lattice parameter $a$ and the oxygen position parameter $u$, as indicated by $d_A = a\sqrt{3}$ $(1/8 + \varepsilon)$ and $d_B = a$ $(1/16 - \varepsilon/2 + 3\varepsilon^2)^{1/2}$, where $\varepsilon = u - 3/8$. Besides, the oxygen parameter $u$ is a function of the oxide composition and its value varied from 0.3889$_5$ ($x = 0$) to 0.3888 ($x = 1$). Interestingly, an ideal spinel structure is characterized by $u = 0.375$. Distances $d_A$ and $d_B$ can also be expressed as a function of the metallic cation molar fraction $X$, $d_A = \Sigma X_A$ (Mi–O)$_A$ and $d_B = \Sigma X_B$ (Mi–O)$_B/2$, where (Mi–O)$_A$ and (Mi–O)$_B$ correspond to the tetrahedral and octahedral distances, respectively. Based on these distance values, the cell parameter $a$ may be calculated, irrespective of the $\varepsilon$ values, using the relationship $a = 2.00995$ $d_A + (5.8182 \, d_B^2 - 1.4107 \, d_A^2)^{1/2}$.

We were able to determine the most probable cationic distribution of the propionic-route oxide as a function of $x$ (Table 4) by using appropriate software and the Ni$^{2+}$–O and Mn$^{n+}$–O distances, where $n$ can be 2, 3, or 4 (37). This distribution is a result of a coherent and overall interpretation of the X-ray diffraction data, conductivity measurements, oxygen and cation chemical analyses, and IR spectroscopy data, considering cation preference for either A or B sites. According to the data from Table 4, when Al is replaced by Ni, Mn$^{4+}$/Mn$^{3+}$ couples will appear at the octahedral sites along with the expected increases of $a$, $\sigma$, and $\mu$ and decrease of $E_a$. Such a decrease of $E_a$ correlates with the increased probability of electron hopping from Mn$^{3+}$ to Mn$^{4+}$ along the conductivity chains Mn$^{3+}$–Mn$^{4+}$–Mn$^{3+}$. The ionic distribution proposed here is reinforced by the similarities between $q_{exp}$ and $q_{calc}$ (Table 4). Ni–Al manganites have relatively high pHz values because the majority species are Al(III) and Ni(II) at their surfaces: pHz for Al$_2$O$_3$ and NiO are 9.1 and 8.0, respectively, while pHz for Mn$_2$O$_3$, Mn$_3$O$_4$, and MnO$_2$ are 2.45, 2.3, and 2.35, respectively. For $x \leq 0.35$, the unbalance in

### TABLE 4
### Effect of $x$ Value on the Ionic Distribution for the $Ni_xAl_{1-x}Mn_2O_4$ System Prepared by the Propionic Route

| $x$ | Ionic distribution | $q$ (eq. mol$^{-1}$) | |
|---|---|---|---|
| | | $q_{exp}$ | $q_{calc}$ |
| 0 | $Mn^{2+}[Al^{3+}_{0.93}Mn^{3+}V^{'''}_{0.07}]O^{2-}_{3.9}V^{\cdot\cdot}_{0.1}$ | 1.0 | 1.0 |
| 0.2 | $Ni^{2+}_{0.01}Mn^{2+}_{0.99}[Al^{3+}_{0.75}Ni^{2+}_{0.19}Mn^{3+}_{0.82}Mn^{4+}_{0.19}V^{'''}_{0.05}]O^{2-}_{3.92}V^{\cdot\cdot}_{0.08}$ | 1.2 | 1.2 |
| 0.35 | $Ni^{2+}_{0.02}Mn^{2+}_{0.98}[Al^{3+}_{0.62}Ni^{2+}_{0.33}Mn^{3+}_{0.69}Mn^{4+}_{0.33}V^{'''}_{0.03}]O^{2-}_{3.95}V^{\cdot\cdot}_{0.05}$ | 1.3 | 1.3$_5$ |
| 0.5 | $Ni^{2+}_{0.1}Mn^{2+}_{0.9}[Al^{3+}_{0.5}Ni^{2+}_{0.4}Mn^{3+}_{0.7}Mn^{4+}_{0.4}]O^{2-}_4$ | 1.4 | 1.5 |
| 0.8 | $Ni^{2+}_{0.12}Mn^{2+}_{0.88}[Al^{3+}_{0.2}Ni^{2+}_{0.68}Mn^{3+}_{0.44}Mn^{4+}_{0.68}]O^{2-}_4$ | 1.8 | 1.8 |
| 1.0 | $Ni^{2+}_{0.28}Mn^{2+}_{0.72}[Ni^{2+}_{0.72}Mn^{3+}_{0.56}Mn^{4+}_{0.72}]O^{2-}_4$ | 2.0 | 2.0 |

*Note.* $V$ = vacancies.

cationic total molar charge with respect to the oxygen charge reflects the nonstoichiometry in oxygen with respect to the stoichiometric formula $Ni_xAl_{1-x}Mn_2O_4$. A similar cationic distribution was obtained for oxides prepared by the oxalic route (not shown here). It is noteworthy that other oxides, such as $M$–Co ferrites ($M$ = Mn, Mo), have been reported as cation-deficient spinels (38, 39).

Based on data from Table 2, a correlation between $x$ and surface properties, such as pHz, i.e.p., and $C_{app}$, can be deduced: the higher the $Mn^{4+}/Mn^{3+}$ value, the lower the pHz, i.e.p., and $C_{app}$ values, supporting the notion of the importance of $Mn^{4+}$ ions in these oxides.

Catalysis of OER (Table 3) correlates clearly with the increase in Mn content and, probably and more precisely, with the increase in $Mn^{4+}$ cation concentration (Table 4). Surface $Mn^{4+}$ cations are commonly viewed as part of the active sites of spinel manganese oxides. Probably these cations, at octahedral sites, would accelerate the oxidation of $OH^-$ ions in cases when no other redox couples were present at this coordination. We have recently detected that Mn inhibited the OER in Teflon-bonded $Mn_xCo_{3-x}O_4$ graphite electrodes since surface manganese is mainly in a trivalent state in these materials (40, 41). The electrocatalytic role of the Ni(III)/Ni(II) couple in $NiCo_2O_4$ spinel has also been reported by us (42). When apparent current densities for $MnCo_2O_4$ and $NiCo_2O_4$ thin films were measured in Refs. (40, 42) under the same conditions (1 M KOH and 25°C), the values obtained were 0.13 and 2.2 mA cm$^{-2}$, respectively. These can be compared with the $j$ value of 3.5 mA cm$^{-2}$ obtained in this work. Further studies on XPS's surface characterization are necessary to discriminate between Mn and Ni effects on the electrocatalytic properties of these electrode materials for OER.

## 5. CONCLUSIONS

Nickel aluminum spinel $Ni_xAl_{1-x}Mn_2O_4$ ($0 \leq x \leq 1$) with high purity and good crystallinity can be prepared from thermal decomposition of oxalates and propionates in the range 800–1,000°C, followed by thermal treatment at 500°C to minimize entropy. All oxides showed the properties of mixed valency oxides of transition elements and conductivities corresponding to electronic transfers by a hopping process, with relatively low activation energies between Mn cations with different valencies. The propionic-route electrodes showed better homogeneity than oxalic route electrodes. Both conductivity and activation energy were influenced by oxygen deficiency at $x < 0.5$. A clear correlation was observed between chemical composition and parameters that characterize oxide/solution interfaces (pHz, i.e.p., $C_{app}$, Rf). Therefore, this work demonstrates that electrocatalysis can be controlled by solid state chemistry, and because the OER rate can be varied according to manganese and nickel content at the octahedral sites of the spinel structure, applications of these type of oxides in electrolyzers and metal/air batteries can be visualized.

## REFERENCES

1. E. J. M. O' Sullivan and E. J. Calvo, in "Reactions and Metal Oxides Electrodes" (R. E. Compton, Ed.), Comprehensive Chemical Kinetics, Vol. 27, p. 247. Elsevier, Amsterdam, 1987.
2. J. L. Gautier, in "Electrocatálisis: Tópicos Especiales" (A. J. Arvía and Marschoff, Eds.), Chap. 12. FECC, Buenos Aires, 1989.
3. E. D. Macklen, *J. Phys. Chem. Solids* **47,** 107 (1986).
4. M. S. Islam and C. R. A. Catlow, *J. Phys. Chem. Solids* **49,** 119 (1988).
5. R. Legros, R. Metz, and A. Rousset, *J. Mater. Sci.* **25,** 4410 (1990).
6. F. C. Romeijn, *Philips Res. Rep.* **8,** 304 (1953).
7. D. B. Ghare and A. P. B. Sinha, *J. Phys. Chem. Solids* **29,** 885 (1968).
8. P. Porta, F. S. Stone, and R. Turner, *J. Solid State Chem.* **11,** 135 (1974).
9. N. Nguyen Cong, P. Chartier, and J. Brenet, *J. Appl. Electrochem.* **7,** 395 (1977).
10. J. Ortiz and J. L. Gautier, *J. Electroanal. Chem.* **391,** 111 (1995).
11. J. L. Gautier, A. Restovic, G. Poillerat, and P. Chartier, *Eur. J. Solid State Inorg. Chem.* **34,** 367 (1997).
12. A. Restovic, G. Poillerat, P. Chartier, and J. L. Gautier, *Electrochim, Acta* **40,** 2669 (1995).
13. P. Nkeng, J.-F. Koenig, J. L. Gautier, P. Chartier, and G. Poillerat, *J. Electroanal. Chem.* **402,** 81 (1996).
14. M. El Baydi, G. Poillerat, J-L. Rehspringer, J. L. Gautier, J. F. Koenig, and P. Chartier, *J. Solid State Chem.* **109,** 281 (1994).
15. J. L. Gautier, A. Restovic, A. Derory, G. Poillerat, and P. Chartier, *Bol. Soc. Chil. Quim.*, **42,** 147 (1997).
16. A. Restovic, G. Poillerat, J. F. Koenig, P. Chartier, and J. L. Gautier, *Thin Solid Films* **99,** 139 (1991).
17. A. C. C. Tseung and H. L. Bevan, *J. Mater. Sci.* **5,** 604 (1970).
18. K. M. E. Miedzinska, B. R. Hollebone, and J. G. Cook, *J. Phys. Chem. Solids* **48,** 649 (1987).
19. J. Ponce, G. Zelada, and J. L. Gautier, *Bol. Soc. Chil. Quim.* **30,** 243 (1990).
20. L. L. Hench and J. K. West , *Chem. Rev.* **90,** 33 (1990).
21. G. Yi and M. Sayer, *Ceram. Bull.* **70,** 1173 (1991).

22. J. L. Gautier, S. Zapata, and S. Barbato, *J. Chim. Phys.* **82,** 421 (1985).
23. D. A. Skoog, D. M. West, and F. J. Holler, *in* "Química Analitica," p. 315. McGraw–Hill, Mexico, 1995.
24. J. O.' M. Bockris and T. Otagawa, *J. Electrochem. Soc.* **131,** 290 (1984).
25. J. L. Gautier, A. Restovic, and P. Chartier, *J. Appl. Electrochem.* **19,** 28 (1989).
26. H. Masuki and T. H. Kamada, *Electrochim. Acta* **91,** 13 (1986).
27. M. H. Mueller, L. Heaton, and K. T. Miller, *Acta Crystallogr.* **13,** 828 (1960).
28. R. R. Heikes and W. D. Johnston, *J. Chem. Phys.* **26,** 582 (1957).
29. R. D. Waldron, *Phys. Rev.* **99,** 1727 (1955).
30. J. Preudhomme and P. Tarte, *Spectrochim. Acta Part A* **27,** 1817 (1971).
31. E. G. Larson, R. J. Arnott, and D. G. Wickham, *J. Phys. Chem. Solids* **23,** 1771 (1962).
32. E. H. L. Dekker and G. D. Reick, *Z. Anorg. Allg. Chem.* **415,** 69 (1975).
33. B. Gillot, M. Kharroubi, R. Metz, R. Legros, and A. Rousset, *Solid State Ionics* **44,** 275 (1991).
34. E. H. L. J. Dekker and G. D. Rieck, *Rev. Int. Houtes Temp. Réfract.* **2,** 187 (1974).
35. V. A. M. Brabers and J. C. J. M. Terhell, *Phys. Status Solid* (*a*) **69,** 325 (1982).
36. P. Poix, *Bull. Soc. Chim. Fr.* **5,** 1085 (1965).
37. A. Paul and S. Basu, *Trans. J. Br. Ceram. Soc.* **73,** 167 (1974).
38. P. Tailhades, Ch. Sarda, P. Mollard, and A. Rousset, *J. Magn. Mater.* **104,** 969 (1992).
39. E. Kester, B. Gillot, L. Bouet, P. Tailhades, and A. Rousset, *Thermochim. Acta* **261,** 209 (1995).
40. E. Ríos, J. L. Gautier, G. Poillerat, and P. Chartier, *Electrochim. Acta* **44,** 1491 (1998).
41. J. L. Gautier, E. Ríos, M. Gracia, J. F. Marco, and J. R. Gancedo, *Thin Solid Films* **311,** 51 (1997).
42. R. N. Singh, M. Hamdani, J. F. Koenig, G. Poillerat, J. L. Gautier, and P. Chartier, *J. Appl. Electrochem.* **20,** 442 (1990).